Observations of hail cores of tornadic thunderstorms with four polarimetric radars

Valery Melnikov[1,2], Dusan Zrnic[2], Donald Burgess[1,2], and Edward Mansell[2]

[1]*The University of Oklahoma, CIMMS, Norman, OK.*

[2] *NOAA/OAR National Severe Storms Laboratory, Norman, OK.*

(Dated: 1 July 2014)

1 Introduction

Supercell thunderstorms typically produce hail. The largest hail is commonly found at the edges of the updrafts, which allow sufficient growth time for hail to reach large sizes (Miller et al. 1988). An algorithm for hail recognition with the single polarization WSR-88D (Weather Surveillance Radar-Doppler) has been in use since early 1990s (Witt et al. 1994). Dual polarization radar capabilities allow measurements of differential reflectivity (Z_{DR}), the correlation coefficient (ρ_{hv}), and differential phase (Φ_{dp}), which deliver additional information about scatterers. Studies by Balakrishnan and Zrnic (1990) of hail producing thunderstorms reveal low Z_{DR} (about 0 dB) and reduced ρ_{hv} (as low as 0.8) in hail cores. These features are explained with tumbling non-spherical hailstones: the correlation coefficient drops because the scatterers are not spherical and Z_{DR} is low because they tumble. Further works reveal variety of hail cases with reflectivities in a wide interval from ~ 30 to over 70 dBZ, with Z_{DR} in the interval from -1 to 3 dB and ρ_{hv} in the interval from 0.4 to 0.9 (e.g., Ryzhkov et al. 2005b; Heinselman and Ryzhkov 2006, Picca and Ryzhkov 2012).

Variations in polarimetric properties in hail cores are explained with variations in the hailstone shape and sizes, their kinematic characteristics (tumbling and precession/rotation), presence of water on hailstones' surfaces, and resonant scattering effects. The polarimetric characteristics of hail are typically explored for a given wavelengths. In this study we analyze data collected with radars operating at different frequencies and observing the same areas of storms (sections 3 and 4) and study dependencies of polarimetric properties upon radar characteristics such as operating frequencies and the system differential phase on transmit (section 5).

2 Radar systems

Tornadic hailstorms developed in central Oklahoma in May 2013 were observed with four polarimetric radars: three WSR-88Ds and a mobile X band system. These are WSR-88D KOUN and KCRI located in Norman, OK (Fig. 1) within a short distance of 230 m from each other. The third WSR-88D was KTLX system located at the azimuth of 53^o and 26 km from KOUN/KCRI. The WSR-88Ds operate at S frequency band. NOXP radar is a 3-cm wavelength system; it was deployed about 100 m from the KOUN's tower for the experiment (Fig. 1). To reduce signal interference between the WSR-88Ds, the radars operate at different frequencies listed in Table 1.

The WSR-88Ds and NOXP employ a polarization configuration with Simultaneous Transmission And Reception (STAR) of horizontally and vertically polarized waves. The NOXP antenna is a scaled clone of the WSR-88D's ones. Both antennas have equal beamwidths of 0.95^o. Due to strong attenuation of 3-cm wavelength radiation in thunderstorm, NOXP is not a good system for observations of hail thunderstorms which is demonstrated in the next section. So the data from the three WSR-88Ds operating at different frequencies have been analyzes. Our main goal of this communication is an analysis of impacts of different radar frequencies and phase characteristics on observed reflectivity Z, Z_{DR}, and ρ_{hv}.

Attenuation of radar waves at S band is significant and has to be corrected for. Corrections for reflectivity (ΔZ) and differential reflectivity (ΔZ_{DR}) in data obtained with the WSR-88Ds in areas between radars and hail cores is made by using measured differential phase Φ_{DP} as follows,

$$\Delta Z = 0.04\ \Phi_{DP,} \quad \Delta Z_{DR} = 0.004\ \Phi_{DP},$$

where ΔZ and ΔZ_{DR} are in dB and Φ_{DP} is in degrees. It is assumed that the medium between hail cores and radar contains raindrops. Values of ΔZ and ΔZ_{DR} are added to measured Z and Z_{DR} because we used the Level II radar data, which are not corrected for attenuation.

Table 1. Operating frequencies of the WSR-88Ds and NOXP.

Radar	Frequency, MHz	Frequency band
KOUN	2705	S
KTLX	2910	S
KCRI	2995	S
NOXP	9410	X

Fig. 1. Locations of WSR-88Ds KOUN and KCRI and the parking spot for mobile NOXP in Norman, OK. MPAR is the Multifunctional Phased Array Radar.

3 . Event 31 May 2013

Radar images of tornado and hail producing thunderstorm observed 31 May, 2013 with the four radars are shown in Fig. 2. The images at lowest antenna elevation of 0.5^o are presented. The storm produced EF3 tornado at the time; the tornado was located in the hook echo area indicated in the figure with '1'. The tornadic area is surrounded with an arc of high reflectivity to the North from the tornado vortex. The area with tornado mesocyclone has low Z_{DR} and the tornadic ball has low ρ_{hv}. The Z_{DR} arc is seen along the inflow edge of the storm. These features are typical for tornadic storms (Kumjian and Ryzhkov 2008, Schwarz and Burgess 2011) and can be seen in images from the three radars.

One can see that X-band radiation experienced severe attenuation: only front areas of the thunderstorm were observed with NOXP. Luckily, the tornado occurred at a cloud fringe close to the radar so it was observed by NOXP. Severe attenuation made Z_{DR} from NOXP negative at the far fringes of observed echoes. Due to tremendous attenuation NOXP's data cannot be used for analyzing hail cores in this event.

An area of strong reflectivity to the North from the tornado mesocyclone did not produce hail on the ground. Large hail with sizes up to 6 cm was produced by the ridge of high reflectivity indicated with number '2' in Fig. 2 (see the top left panel). Maximal reflectivity values from these two areas were about 63-67 dBZ, i.e., about the same. To compare radar polarimetric characteristics from the areas, values of Z_{DR} and ρ_{hv} have been presented as function of reflectivity for the reflectivity values larger than 40 dBZ. This threshold have been chosen since probability of hail increases sharply for reflectivity values exceeding 50 dB (Witt et al. 1994) but it is known that hail can be produced in areas with reflectivities as low as 30 dB.

Figs. 3(a,b) present the mean Z_{DR} and ρ_{hv} as a function of reflectivity for area '1'. Similar graphs for area '2' are shown in Figs. 3(c,d). The mean values are indicated with brackets, i.e., $<Z_{DR}>$ and $<\rho_{hv}>$. In Figs. 3(a,b) one can see that $<Z_{DR}>$ values increase with Z. This feature is opposite to usual expectations that Z_{DR} and ρ_{hv} should decrease with Z in hail areas. It is also seen that $<Z_{DR}>$ from KOUN exceed the values from KTLX by 1 dB, which is significant and cannot be explained with miscalibrations of differential reflectivity in the systems. The values of ZDR are high and reach 3-4 dB for very large Z. Such a behavior can be explained with the presence of small hailstones having torus water films. Values of $<\rho_{hv}>$ as function of Z from the three radars do not exhibit similar behaviors (Fig. 3b): the correlation coefficient (CC) from KOUN and KCRI increase with Z whereas CC from KTLX drops at Z > 57 dB.

In area '2' (the hail core), one can see that $<Z_{DR}>$ values increase with Z for KOUN and remains rather constant for KCRI and KTLX (Fig. 3c). The data from all radars exhibit rather high Z_{DR} values. The values of ρ_{hv} are in an interval from 0.94 to 0.98 (Fig. 3d); The mean CC from KOUN increase with Z whereas other two radars show rather a decrease. One more feature should be noticed in Fig. 3: the maximal reflectivity values from KOUN is noticeably larger than the one for other radars. In Figs. 3ab, this difference reaches 7-8 dB.

Fig. 4 presents polarimetric fields from the four radars at about 00:24 UTC on June 1, 2013 when a giant hail was observed on the ground in area '2'. An example of a hailstone is shown in Fig. 5 and its location is shown in the left top panel of Fig. 4 with a circle (to the north-west from '1'). The largest reported hailstone sizes were about 7 cm. X band radiation experienced severe attenuation as in the previous case therefore the southern thunderstorm's fringe was only visible for NOXP radar.

Fig 6 presents the mean $<Z_{DR}>$ and $<\rho_{hv}>$ as functions of reflectivity as in Fig. 3. Maximal reflectivities in area '2' (left bottom panels in Fig. 6) were about the same whereas in area '1' (Figs. 6 ab), maximal reflectivity from KOUN is 5 dB higher than the values from KCRI and KTLX. One can see that in area '1", $<Z_{DR}>$ increase with Z and reach 3-4 dB at maximal Z. This is similar to Fig. 3a. The difference between $<Z_{DR}>$ from KOUN and KTLX is about 1 dB. The values of $<\rho_{hv}>$ from KOUN show some increase with Z whereas the values from other radars remain rather the same (Fig. 6b).

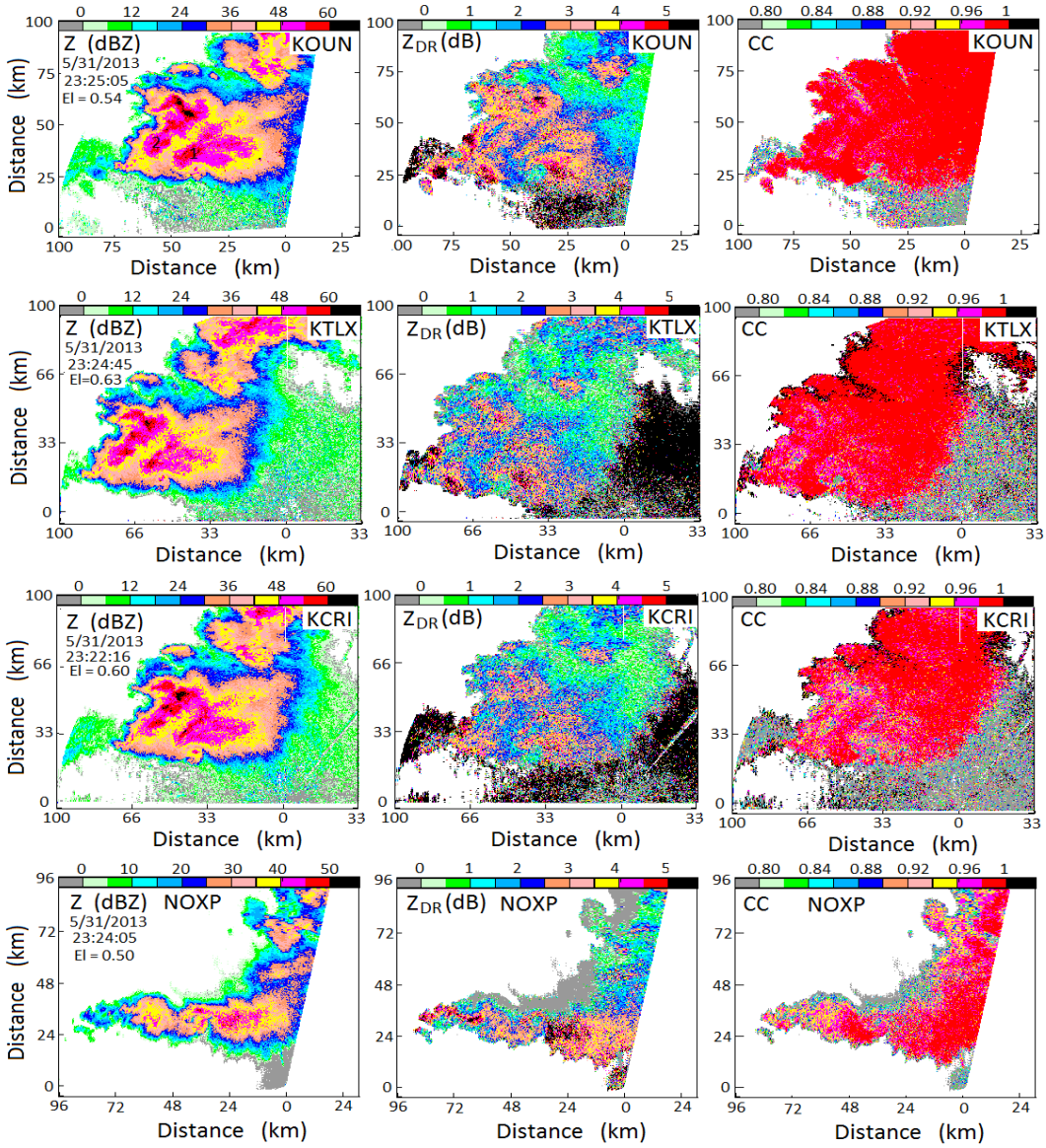

Fig. 2. Polarimetric fields of tornadic thunderstorm on May 31, 2013 at about 23:24 UTC. The data were collected with KOUN, KTLX, KCRI, and NOXP at the time of strong EF3 tornado near El Reno, OK.

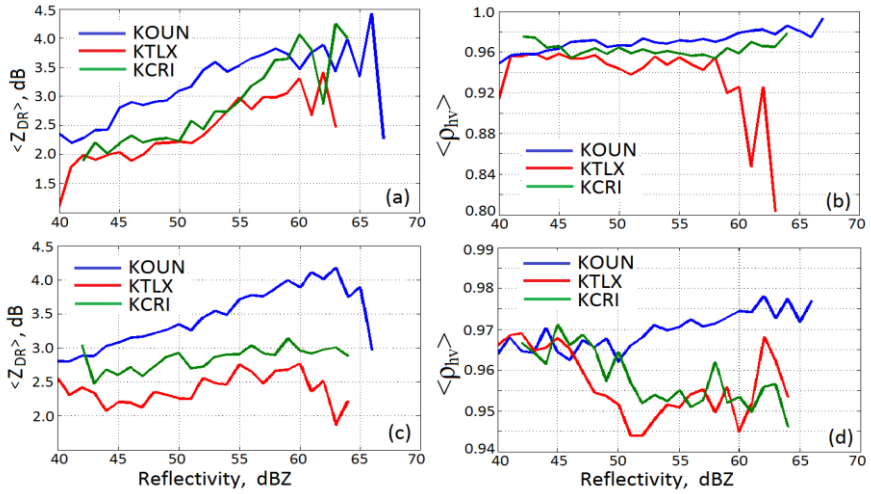

Fig. 3. (a): The mean Z_{DR} as a function of reflectivity for an area of high reflectivity indicated with "1" in the left top panel of Fig. 2. (b): Same as in (a) but for the mean correlation coefficients. (c,d): Same as in (a,b) but for high reflectivity core designated with "2" in the left top panel of Fig. 2.

In area '2' (giant hail), there is no definite dependence $<Z_{DR}>$ upon Z: $<Z_{DR}>$ remain about the same for each radar but difference between curves for KOUN and KTLX remains about 1 dB for Z > 50 dB (Fig. 6c). The values of $<\rho_{hv}>$ from KOUN do not show big difference in areas '1' and '2' whereas for the other two radars, $<\rho_{hv}>$ values exhibit drop from about 0.96 to 0.93-0.94 at Z < 50 dB (Fig. 6d). At Z > 50 dB, one can see increase in $<\rho_{hv}>$ for all three radars, which is against usual expectations of decreased CC in areas with large hail.

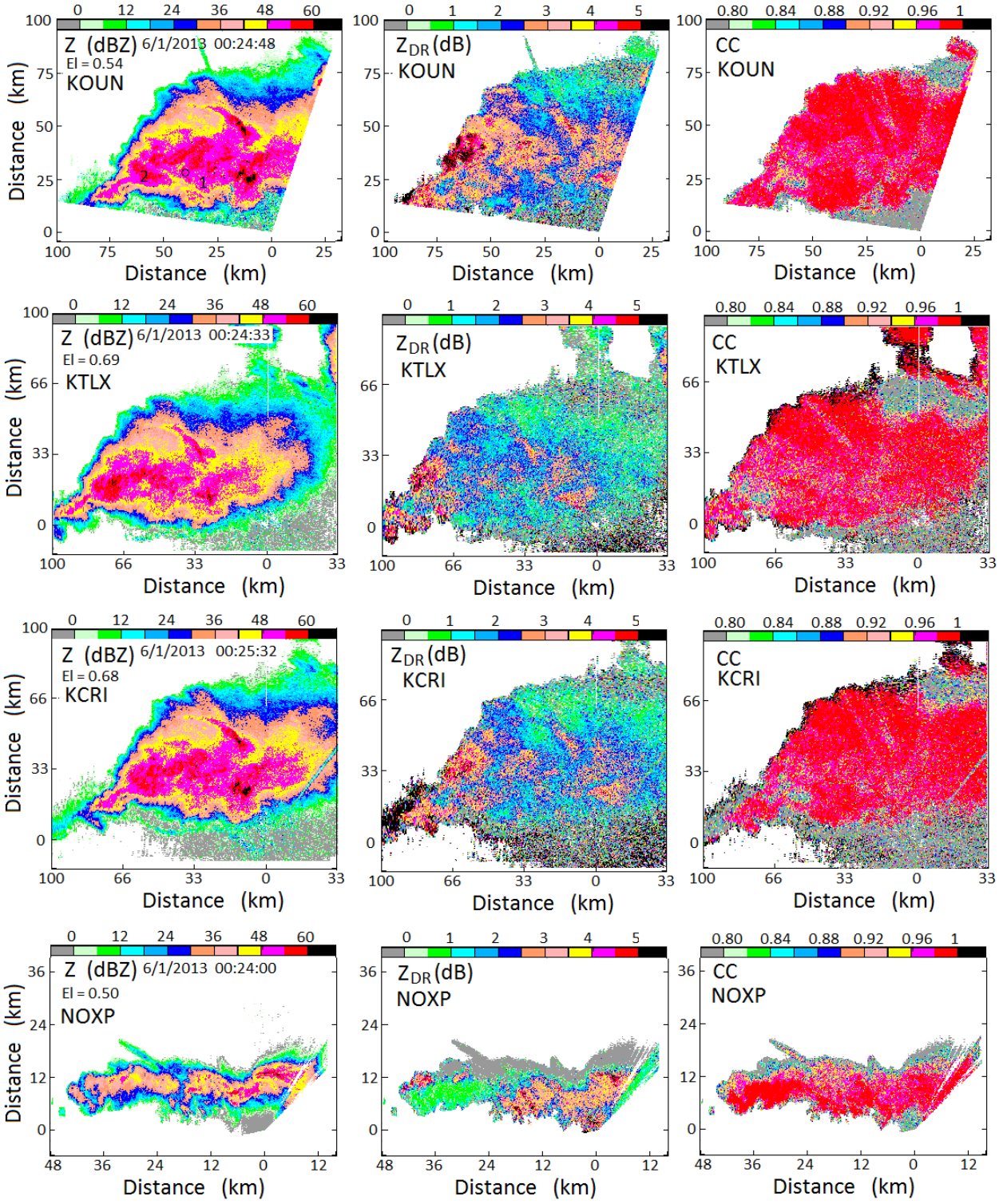

Fig. 4. Polarimetric fields collected with KOUN, KTLX, KCRI, and NOXP on June 6, 2013 at 0024 about the time when giant hail on the ground was observed. The location of giant hail is shown with a circle in the left top panel (to the north-west from '1').

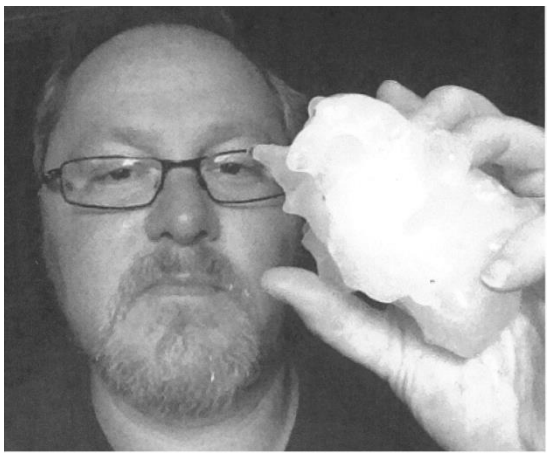

Fig. 5. A giant hailstone picked up by Mr. J. Coleman in city of El Reno, OK 6/1/2013 at about 0025 Z. Courtesy of Mr. J. Coleman and Mr. R. Doviak.

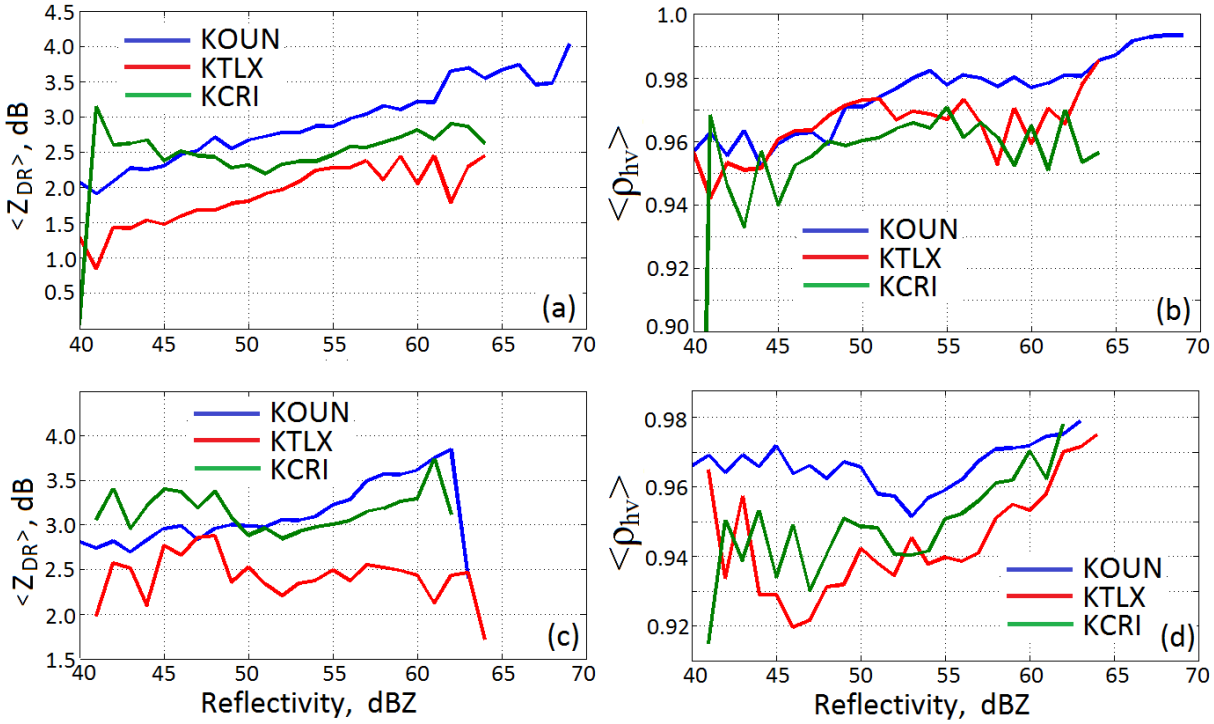

Fig. 6. (a): The mean Z_{DR} as a function of reflectivity for an area of enhanced reflectivity in area "1'. (b): Same as in (a) but for the mean correlation coefficients. (c,d): Same as in (a,b) but for high reflectivity core designated with "2" in the left top panel of Fig. 4.

4. Event 19 May 2013

Fig. 7 presents polarimetric fields collected 19 May, 2013 in tornadic thunderstorm devastated City of Moor, OK. The tornado was spawned in the hook echo in the southern fringe of radar echo. Hail with sizes of 2 cm was observed in the area of strongest reflectivity.

In Fig. 8, the mean $<Z_{DR}>$ and $<\rho_{hv}>$ as functions of Z are shown. Again, maximal reflectivity from KOUN is 5 dB larger than those from KTLX and KCRI and the difference in $<Z_{DR}>$ from KOUN and KTLX is about 1 dB for Z < 60 dBZ. Values of $<\rho_{hv}>$ are noticeably lower than those for the previous event.

The following conclusion can be drawn from data collected from the two tornadic cases.

- Maximal reflectivity values from KOUN are frequently larger than those from other two WSR-88Ds, i.e., KTLX and KCRI. It should be noted that KOUN operates at lower frequency than KTLX and KCRI.
- Z_{DR} values from KOUN are larger than those from KTLX by about 1 dB, which is a substantial number that cannot be attributed to miscalibration of differential reflectivities in the systems.
- The correlation coefficients did not show noticeable drops in areas with giant hail. There seems to be no indications on drops in $<\rho_{hv}>$ with increasing Z. Dependences of $<\rho_{hv}>$ on radar frequencies have not been revealed.

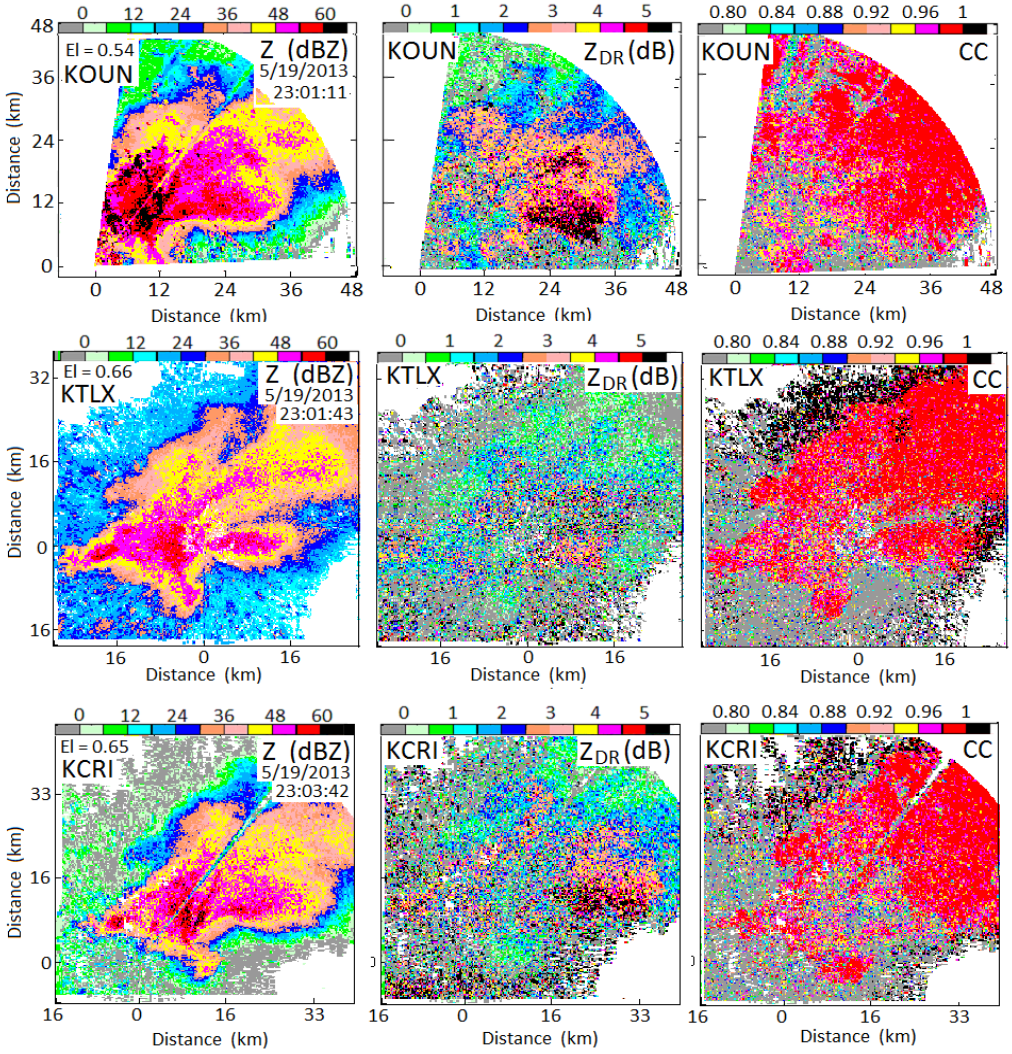

Fig. 7. Polarimetric fields collected with KOUN, KTLX, and KCRI on May 19, 2013 at about 23:01 UTC.

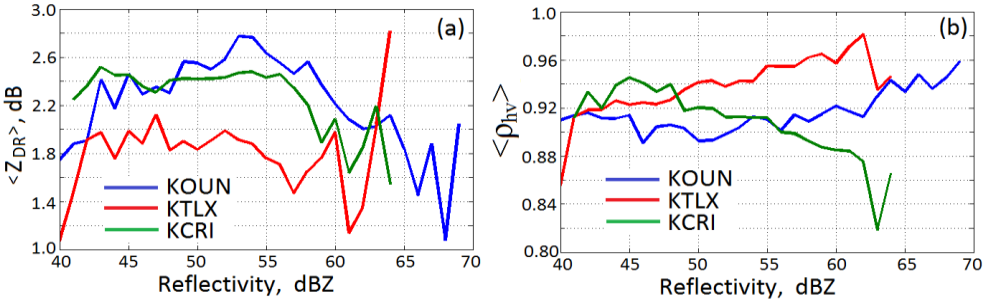

Fig. 8. (a): The mean Z_{DR} as a function of reflectivity for event 19 May, 2013. (b): Same as in (a) but for the mean correlation coefficients.

5 Impacts of radar parameters on hail recognition

The WSR-88D radars operate at S frequency band 2700 – 3000 MHz. Adjacent WSR-88Ds operate at slightly different frequencies to reduce interference. Experiments conducted on two WSR-88Ds with different frequencies show different reflectivity values in hail cores (Melnikov et al. 2011). So one of radar parameters that impact measured reflectivity and differential reflectivity is radar frequency. Another radar parameter is differential phase on transmit ψ_t; we show its impacts on the differential phase upon scattering and correspondingly on the correlation coefficient (section 5.2).

5.1. Impacts of radar frequency

Carrier frequencies of adjacent WSR-88D radars are offset to reduce signal interference. Changes in carrier frequencies slightly change radar parameters such as the antenna beamwidth, waveguide losses, and receiver sensitivity. An automatic calibration procedure, running on all radars, brings reflectivity values to the same level with accuracy of 1 dB. The radar

calibration procedure is based on basic engineering principles and assumes same scattering properties of weather echoes. One of the missions of the WSR-88Ds is precipitation measurement. The maximal stable size of raindrops is 6 mm which is small compared to the wavelength, i.e., 10 cm, so that the Rayleigh approximation for scattering properties are often used for rain. Sizes of hailstones can be a few centimeters and the Rayleigh approximation cannot be used in calculation of their scattering properties. For spherical hailstones, Mie theory is used. It follows from the theory that the radar cross section is an oscillating function of the diameter and wavelength so that radar backscattering cross sections and correspondingly reflectivities are different at different wavelengths. This is frequently called the resonant effect highlighting strong oscillations of scattering cross sections as functions of size or wavelength. This effect is used for hail detection with a two-wavelength radar, 3- and 10-cm, i.e., at X- and S-bands (Atlas and Ludlum 1961, Eccles and Atlas 1971, Doviak and Zrnic 2006, section 8.5.1) and at C- and S-bands (Féral et al. 2003), i.e., at highly diverse frequencies.

For radars at a narrow frequency band, it is assumed that small deviations of carrier frequencies do not change radar cross section substantially so that reflectivities are the same for the band. Melnikov et al. (2010) analyzed this assumption for rain and hail for the WSR-88D's frequency band and showed that the resonant effect can cause a noticeable difference in reflectivity measured with adjacent WSR-88Ds. This means that adjacent radars, that use slightly different carrier frequencies, will measure different reflectivity values due to the resonant effect if hail is present.

The difference in measured reflectivity values at wavelengths λ_1 and λ_2 is

$$Z_{\lambda 1} - Z_{\lambda 2} = 10\log[\int \sigma(D,\lambda_1)N(D)dD / \int \sigma(D,\lambda_1)N(D)dD], \quad (1)$$

where $N(D)$ is the size distribution, i.e., the number of particles with diameter D in the unit volume and $\sigma(D,\lambda)$ is the backscatter cross section of the scatterer. This difference depends on the wavelengths and sizes of hydrometeors. To calculate radar reflectivity for hailstones, we utilized the T-matrix method (Mischenko et al. 2002).

If hail is present in the radar volume, the difference of radar cross sections can reach several dB. Dry hailstones do not contain water on their surface. If there is a water film on the surface of a hailstone, such hailstones are usually called wet. Spongy hailstones consist of a mixture of ice and water.

Size distributions $N(D)$ of hailstones can be of different shapes. Smaller sizes have been represented by an exponential function or a gamma function (Cheng and English 1983, Federer and Wladvogel 1975) but large sizes often seem to have narrow distributions centered on the mean (Ziegler et al. 1983). Thus we consider different $N(D)$. Results for a uniform distribution between *Dmin* and *Dmax* with *Dmax* - *Dmin* = 1 cm are presented in Fig. 9(a) as a function of *Dmax*. It is seen that the reflectivity difference can exceed 2 dB for hailstones with diameters larger than 3.5 cm and reaches 6 dB at *Dmax* = 4.5 cm for wet hailstones. For exponential distributions, shown in Figs. 9(b), the Z difference can be 2 dB for *Dmax* in the interval 3.5 to 5 cm. In our calculations, we used Λ=0.3 (Doviak and Zrnic 2006, section 8.1.3) in $N(D) = N_0 \exp(-\Lambda D)$.

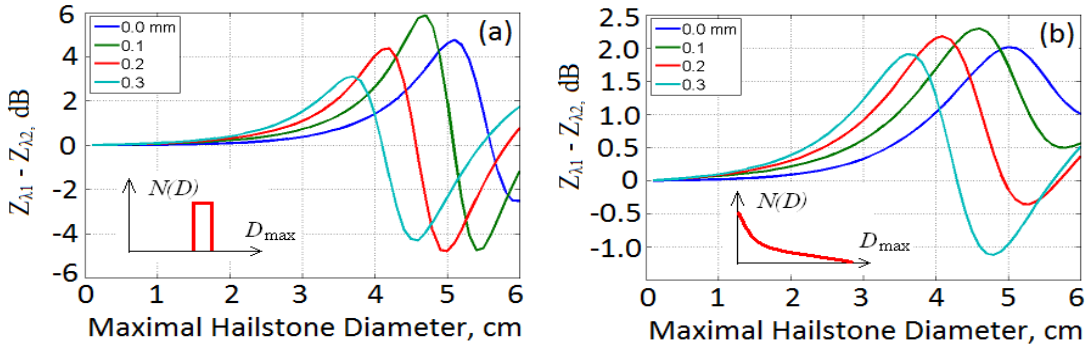

Fig. 9. (a): The difference of reflectivity values of spherical hailstones at two wavelengths corresponding to KOUN (λ=11.1 cm) and KCRI (λ=10.0 cm for two forms of size distributions shown in the inserts. The thickness of water films on hailstones is indicated in the legends.

Two general conclusions can be deduced from Fig. 9. 1) Resonant effects can produce a reflectivity difference at close wavelengths as high as 6 dB in a large interval of hailstones diameters from 3.5 to 5 cm. 2) The reflectivity difference can be positive and negative; it is mainly positive for hailstones with diameters smaller than 4.5 cm and it is mainly negative for larger diameters. From these conclusions we deduce that if the hailstone diameter is smaller than 4.5 cm, KOUN reflectivity values can exceed reflectivity values from KCRI. This could explain the first observed feature that was stated in the end of section 2.

Radar observations show that hail can have positive and negative Z_{DR}. Usually positive Z_{DR}, is associated with oblate hailstones falling with the major axis being about horizontal. Negative Z_{DR} is usually associated with conical hailstones falling with the major axis being vertical. Resonant effects make this consideration more complicated: nonspherical scatterers experience different resonances at different dimensions. In Fig. 10(a) for oblate ice spheroid, one can see that oblate scatterers produce negative Z_{DR} for diameters larger than about 50 mm. A similar feature exhibits prolate hailstones (Fig. 10c). This is in contrast to rain wherein oblate raindrops produce positive Z_{DR} only. The difference of Z_{DR}, measured at two wavelengths remains close to zero for prolate and oblate hailstones with sizes less than 5 cm. Thus differences in Z_{DR} measured from two WSR-88Ds point to the presence of very large hailstones with diameters larger than 5 cm. This could explain the second observed issue stated in the end of section 2.

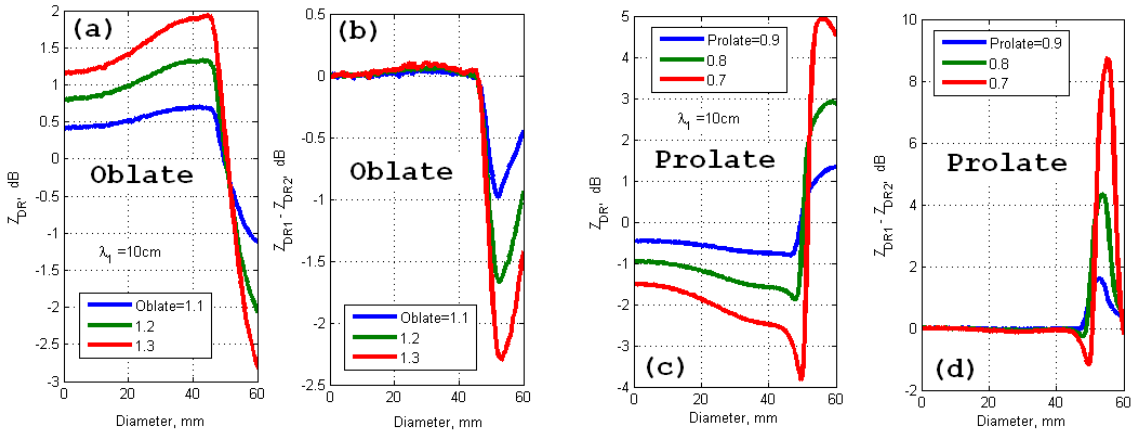

Fig. 10. (a): Differential reflectivity of oblate ice spheroids with oblateness 1.1, 1.2, and 1.3 and (b) the difference of Z_{DR} at two wavelengths corresponding to KOUN (λ=11.1 cm) and KCRI (λ=10.0 cm). (c) and (d) same as in (a) and (b) but for prolate spheroids.

5.2. Impacts of differential phase on transmit

In the STAR radars, signal paths in the two radar channels with horizontally and vertically polarized waves are different so the transmitted and received waves acquire hardware phase shifts on transmit, ψ_t, and on receive, ψ_r. A medium with nonspherical scatterers shifts the phase between the polarized waves by the propagation differential phase Φ_{DP} and differential phase upon scattering δ so that the measured phase shift is $\psi_{dp} = \psi_t + \psi_r + \Phi_{DP} + \delta$. It can be shown that the phase in receive ψ_r does not affect differential reflectivity and correlation coefficient. In contrast, phase ψ_t affects Z_{DR} and ρ_{hv}.

Large hailstones frequently have nospherical shape that means they do not tumble randomly in the air. To acquire nonspherical shapes, hailstones should precess in the air, most likely. Such preceesing can lead to positive Z_{DR} which are observed in hail cores frequently. Precessing affects the differential phase upon scattering and correlation coefficient. The differential phases upon scattering as functions of the azimuthal angle (viewing angle) are shown in Fig. 11a for different ψ_t. The hailstone was modeled with a wet prolate spheroid with the maximal size of 4 cm and axis ratio (width/length= *b/a*) of 0.8. It is seen that ψ_t affects δ significantly. Fig. 11b presents dependences of ρ_{hv} upon ψ_t for different *b/a*. The hailstones are assumed to precess around the vertical axis with the mean canting angle of 30°. Zero canting angle corresponds to rotation on the horizontal plane. One can see that the incident differential phase affects ρ_{hv} significantly.

The incident differential phase is the sum $\psi_t + \Phi_{DP}$. Since this phase depends upon Φ_{DP} its impact on measured differential phase and ρ_{hv} can be different for the same hail core observed from different directions having different Φ_{DP}. Fig. 11b can be used to explain the third issue observed in the events (sections 3 and 4) and stated in the end of section 2: the incident phases for the three WSR-88Ds can be different due to different ψ_t, which can lead to different measured correlation coefficients.

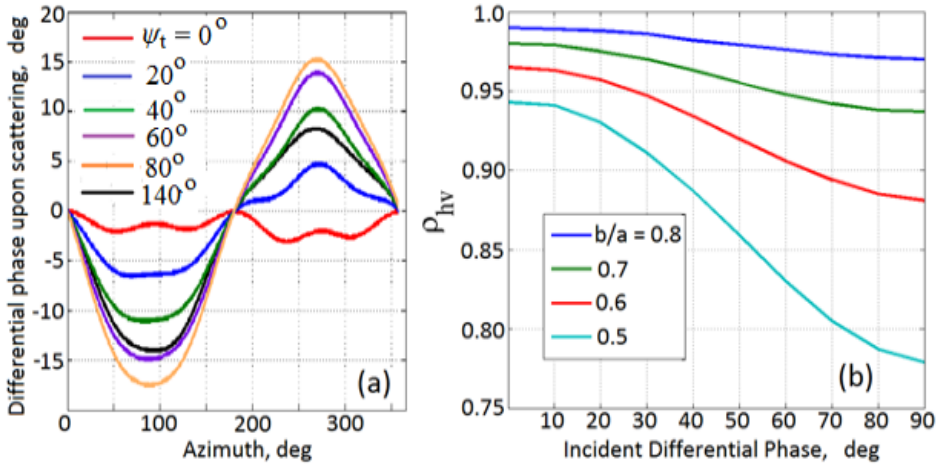

Fig. 11. (a): Differential phase upon scattering by a prolate wet hailstone precessing/rotating over azimuth as a function of azimuth and the incident differential phase ψ_t. The maximal size of the hailstone is 3 cm, the axis ratio is 0.8, and the mean canting angle of precession is 30°. (b): The correlation coefficient for rotating prolate wet hailstones as in (a) as a function of ψ_t and the axis ratio b/a.

6. Conclusions

Our observations of tornadic hailstorms showed severe attenuation of X band radiation; in the events in May 2013 it was so severe that radiation did not reach the hail cores (Figs. 2,4). Therefore data in the hail cores were available only from three S band radars, i.e., KOUN, KTLX, and KCRI.

We have analyzed data collected with three S band radars in the same areas of high reflectivities in the thunderstorms and observed differences in radar variables (sections 3 and 4): reflectivity values, Z_{DR} and ρ_{hv} are different for radars operating at different frequencies. Our calculations show that the difference in frequency about 200 MHz can change reflectivity and Z_{DR} by a few dB in areas containing hail (section 5.1). This effect is a manifestation of resonant nature of scattering by hailstones.

The system differential phase in transmit can alter measured ρ_{hv} for radars with the STAR polarimetric configuration implemented in the WSR-88Ds (section 5.2). This effect is a consequence of depolarization of signals scattered by nonspherical hailstones. Therefore measured correlation coefficients can be different for two radars operating at the same frequency but having different system differential phase on transmit.

References

Atlas, D., and F. H. Ludlum, 1961: Multi-wavelength radar reflectivity of hailstorms. *Quart. J. Roy. Meteor. Soc.*, **87,** 523–534.

Balakrishnan, N., and D.S. Zrnic, 1990: Use of polarization to characterize precipitation and discriminate large hail. *J. Atmos. Sci.*, **47,** 1525-1540.

Burgess, D.W., V. Melnikov, D. Priegnitz, R. A. Brown, P. Heinsleman, E. Mansel, and V. Wood , 2014: Tornadic supercells in central Oklahoma on May 19, 20, and 31 of 2013: NSSL radar data. *94-th AMS annual meeting. Special Symposium on Severe Local Storms.* Atlanta, GA, AMS.

Cheng, L., and M. English, 1983: A relation- ship between hailstone concentration and size. *J. Atmos. Sci.* **40,** 204-213.

Doviak, R. J. and D. S. Zrnic, 2006: *Doppler radar and weather observations*, 2nd ed., Dover Publications, 562 pp.

Eccles, P. J., and D. Atlas, 1973: A dual-wavelength radar hail detector. *J. Appl. Meteor.*,**12,** 847–854.

Federer, B., and Wladvogel, 1975: Hail and raindrop size distributions form a Swiss multicell storm. *J. Appl. Meteor.,* **14,** 91-97.

Féral, L., H. Sauvageot, and S. Soula, 2003: Hail detection using S and C-band radar reflectivity difference. *J. Atmos.Oceanic Technol.*, **20,** 233–248.

Heinselman, P.L., and A.V. Ryzhkov, 2006: Validation of polarimetric hail detection. *Weather and Forecasting*, **21,** 839-850.

Kumjian, M.R., and A.V. Ryzhkov, 2008: Polarimetric signatures in supercell thunderstorms. *J. Appl. Meteor. Climat.*, **48,** 1940 - 1961.

Melnikov, V., R. Lee, and N. Langlieb, 2010: Hail reflectivity signatures from two adjacent WSR-88Ds: carrier frequency and calibration issues. *26th Conference on Interactive Information and Processing Systems (IIPS) for Meteorology, Oceanography, and Hydrology***.** Phoenix, AZ, AMS. https://ams.confex.com/ams/90annual/webprogram/Paper161721.html

Miller, L.J., J.D. Tuttle, and C.A. Knight, 1988: Airflow and hail growth in a severe Norther High Plains supercell. *J. Atmos. Sci.*, **45,** 736-762.

Mischenko M. I., L.D. Travis, and A.A. Lacis, 2002: *Scattering, Absorbtion, and Emission of Light by Small Particles.* Cambridge University Press, 228 pp.

Picca, J., A. Ryzhkov, 2012: A dual-wavelength polarimetric analysis of the 16 May 2010 Oklahoma City extreme hailstorm. *Mon. Wea. Rev.*,**140**, 1385–1403.

Ryzhkov, A.V., T. J. Schuur, D. W. Burgess, and D. S. Zrnic, 2005a: Polarimetric tornado detection. *J. Appl. Meteor.*, **44,** 557-570.

Ryzhkov, A.V., T.J. Schuur, D.W. Burgess, P. L. Heinselman, S. E. Giangrande, and D. S. Zrnic, 2005b: The joint polarization experiment. *Bull. Amer. Meteor. Soc.*, **86,** 809-824.

Schwarz, C.M. and D.W. Burgess, 2011: Supercell polarimetric signatures at X-Band: Data from VORTEX2. Extended Abstracts, *35th Conf. Radar Meteorol.*, AMS, http://ams.confex.com/ams/35Radar/webprogram/Paper191298.html]

Witt, A., M. D. Eilts, G. J. Stumpf, J. T. Johnson, E. De W. Mitchell, K. W. Thomas, 1998: An Enhanced Hail Detection Algorithm for the WSR-88D. *Wea. Forecasting*, **13**, 286–303.

Ziegler C.L., P.S. Ray, and N. C. Knight, 1983: Hail growth in an Oklahoma mutlicell storm. *J. Atmos. Sci.* **40,** 1768-1791.